Experimental Analysis of Floc Size Distribution under Different Hydrodynamics in a Mixing Tank

Denis Bouyer and Alain Liné
LIPE–INSA, 31077 Toulouse Cedex 4, France

Zdravka Do-Quang
ONDEO Services, 78230 Le Pecq, France

DOI 10.1002/aic.10242
Published online in Wiley InterScience (www.interscience.wiley.com).

The goal of this report is to analyze the relationship between characteristic floc size and hydrodynamics in a mixing tank. The first question addressed concerns the relation between an average floc size and the viscous dissipation rate of kinetic energy. A first series of flocculation experiments were conducted in a mixing tank with two impellers (a Rushton turbine and a Lightnin A310 impeller) for equivalent dissipated power conditions. The average floc size is shown to depend on the global dissipation rate; it does not depend on the impeller type. However, the floc size distributions are significantly different for each impeller. The second question addressed concerns the dependency of the floc size on the history of mixing. A second series of experiments consisted of flocculation, breakup, and reflocculation stages. These experiments showed that the average floc sizes are similar after flocculation or reflocculation steps, but, once again, the floc size distributions can be very different with different impellers. The flocculation phenomena analyzed in this study mainly occur in the viscous subrange, with maximum floc size on the order of Kolmogorov microscale. © 2004 American Institute of Chemical Engineers *AIChE J,* 50: 2064–2081, 2004

Keywords: flocculation, floc size distribution, hydrodynamics, dissipation rate of kinetic energy, image processing, mixing

Introduction

In water treatment plants, the flocculation process is used to remove colloidal matter by chemical means. In natural water resources, there is a large amount of colloidal matter that cannot be easily removed by classical separation processes. Pretreatment of colloidal particles is necessary to enhance separation. A classical pretreatment method is the chemical treatment of colloids. Different kinds of flocculants (mineral salts or organic polymers) can be added to the water to be treated, thus enhancing colloid aggregation and making the separation of larger flocs easier. This coagulation/flocculation step is a major process in drinking water treatment plants. The prediction of the optimum coagulant dose is the crucial question for two basic reasons: (1) coagulant overdosing can lead to high operating costs and risks leading to problems with public health concerns and (2) underdosing the coagulant can lead to low treatment efficiency and insufficient removal of solid particles in water treatment plants. Such problems can lead to the failure to meet water quality standards. The new stringent regulations on the acceptable residual coagulant level in the distributed water impose a very strict control of any remaining aluminum or ferric salt residuals. Water treatment facilities will have (or are having) trouble meeting the new stringent regulations, and they can do so only by first developing a fundamental understanding of the flocculation. A better knowledge of both hydrodynamic and colloid chemistry is thus needed.

In water treatment plants, coagulants such as aluminum

Correspondence concerning this article should be addressed to D. Bouyer at bouyer@insa-tlse.fr. A. Liné's e-mail address is line@insa-tlse.fr..

sulfate or ferric chloride are injected to produce hydroxide flocs that are several hundred microns in size. Mixing is a key parameter to performing hydroxide floc aggregation, as shown in the next paragraphs.

The goal of this report is to analyze the relationship between floc size and hydrodynamics. Classically, the average floc size is related to the Kolmogorov microscale of turbulence (Akers, 1987; Biggs and Lant, 2000; Wiesner 1992). Analysis of the literature will show that, surprisingly, the floc size distribution is rarely reported. One of the key points of the present work is the description of the variation with time of both the average floc size and the floc size distribution during orthokinetic flocculation, under different hydrodynamic conditions.

Flocculation steps

Flocculation of colloidal matter can be divided into two steps:

(1) A first step corresponds to the perikinetic coagulation: the challenge is to disperse a coagulant as fast as possible, under efficient mixing, to destabilize colloid matter contained in the water.

(2) A second step corresponds to the orthokinetic flocculation: the challenge is to make individual flocs collide to create larger flocs that will be more easily removed from raw water. In the present study, the first step will not be studied in detail, but it is assumed not to be the limiting step of the process: the coagulant dosage was optimized based on previous experiments conducted in the jar (jar test). In addition, both intensity and duration of the mixing phase imposed during the perikinetic stage were optimized to perform efficient dispersion of the coagulant in the jar. In the experimental portion of the research, special attention was paid to physicochemical conditions, to efficiently destabilize all the colloidal matter.

This report focuses on the orthokinetic step, in which the balance between agglomeration and breakup of flocs controls the floc size distribution.

Characteristic phenomena of hydrodynamics and turbulence

This section reviews flocculation mechanisms and characteristic scales of hydrodynamics and turbulence, with respect to flocculation, in terms of aggregation and breakup. Indeed, the characteristic floc size can be related to the equilibrium between aggregation and breakup. This equilibrium depends on the aggregate strength and on the hydrodynamic stress. We will first review phenomena of hydrodynamics and then those of aggregation and breakup.

Hydrodynamics of Agitated Tanks. The Reynolds number (Re) is defined as

$$\mathrm{Re} = \frac{ND^2}{\nu} \tag{1}$$

where N is the impeller rotation frequency (T^{-1}), D is the impeller diameter (L), and ν is the kinematic viscosity of the fluid (L^2T^{-1}).

Hydrodynamics in a tank is characterized by the power number, defined as

$$N_P = \frac{P}{\rho N^3 D^5} \tag{2}$$

where P is the power dissipated in the tank (ML^2T^{-3}) and ρ is the density of the fluid (ML^{-3}). The power number characterizes the amount of power input into the tank for moving the impeller (diameter D) at a rotational speed N.

Given the volume (V) of liquid in the tank, the power number corresponds to a volume average of the dissipation rate of kinetic energy equal to

$$\langle \varepsilon \rangle = \frac{P}{\rho V} \tag{3}$$

A parameter mainly used in water treatment is the mean velocity gradient (G), defined as

$$G = \sqrt{\frac{P}{\mu V}} \tag{4}$$

where G is the velocity gradient (T^{-1}) and μ is the dynamic viscosity of the fluid ($ML^{-1}T^{-1}$). One can easily derive the equivalent expression

$$G = \sqrt{\frac{\langle \varepsilon \rangle}{\nu}} \tag{5}$$

The velocity gradient is mainly used to determine floc size distributions with population balance modeling (Ducoste, 2002; Duscote and Clark, 1998; Hounslow, 1988; Spicer and Pratsinis, 1996), and it often corresponds to the only hydrodynamic parameter taken into account (Lartiges, 1994; Oles, 1992; Spicer et al, 1998; Wiesner, 1994) One of the questions to answer is whether this global velocity gradient is in itself sufficient to estimate the floc size. Actually, aggregation of flocs is related to collision rate. Because the flocs have a density close to that of water, there is almost no settling, so the flocs follow the fluid motion and thus collision is induced by local velocity gradients within the fluid. The velocity gradient can be expressed in terms of the velocity difference between two points separated by the distance r. It corresponds exactly to the physical meaning of the root mean square (rms) of turbulent velocity $\sqrt{u'^2(r)}$, which is developed below.

Turbulent Scales. The turbulence in the tank can be analyzed in terms of characteristic length and time scales. In any local position in the tank, two length scales are significant:

(1) The Taylor macroscale Λ is an integral scale for the energy-containing eddies. It corresponds to eddies that absorb the kinetic energy from the mean flow. In the region close to the impeller, these large eddies are related to the size of the impeller. Far from the impeller, these eddies are related to the size of the tank.

(2) The Kolmogorov microscale η is the smallest size of eddies. It corresponds to eddies that dissipate the turbulent kinetic energy by viscous dissipation.

The mechanism that transfers energy from the large scale eddies to the small scale eddies is the vortex stretching.

Two Eulerian time scales are also significant in analyzing turbulent flows:

(1) The eddy turnover time τ_E

(2) The Kolmogorov time microscale τ_K

The eddy turnover time measures the time necessary to reduce the size of the eddies, from the large scale (Λ) to the small scale (η). It is thus a measure of the time necessary to transfer energy from the large scale (Λ) to the small scale (η), and consequently a measure of the vortex stretching time scale.

The Kolmogoroff length microscale η is defined by

$$\eta = \left(\frac{\nu^3}{\varepsilon}\right)^{1/4} \tag{6}$$

where ε is the local viscous dissipation rate of turbulent kinetic energy. The Kolmogorov time microscale τ_K is written as

$$\tau_K = \left(\frac{\nu}{\varepsilon}\right)^{1/2} \tag{7}$$

The eddy turnover time is written as

$$\tau_E = \frac{\Lambda}{\sqrt{k}} \approx \frac{k}{\varepsilon} \tag{8}$$

where k is the local turbulent kinetic energy.

In these experiments, the floc size d ranges from the viscous dissipation subrange ($d < 3$–$10\ \eta$) to the inertial subrange ($d > 25\ \eta$). It is thus necessary to define the hydrodynamic stresses corresponding to these turbulent scales.

The distribution of the turbulent kinetic energy over a range of wavenumber is given by

$$\overline{[u'(r)]^2} = \int_k^\infty E(k', t)dk' \tag{9}$$

where u' is the instantaneous turbulent velocity fluctuation, r is a turbulent length scale, $k \sim 1/r$ is the associated wavenumber and $k < k' < \infty$ stands for the turbulent scale smaller than r.

Following Thomas (1964), the energy spectrum function (E) can be expressed as:

For $r < \eta$ (viscous subrange)

$$E(k, t) = C_1 \frac{\varepsilon}{k^3} \nu \tag{10}$$

For $r > \eta$ (inertial subrange)

$$E(k, t) = C_2 \varepsilon^{2/3} k^{5/3} \tag{11}$$

The classical values of the constants are $C_1 = 0.73$ according to Hinze (1959) and $C_2 = 4/15$ according to Obukhoff (1951). After integration (Thomas, 1964), Eq. 9 becomes

For $r < \eta$ (viscous subrange)

$$\overline{[u'(r)]^2} = \frac{C_1}{2} \frac{\varepsilon}{\nu} r^2 \tag{12}$$

For $r > \eta$ (inertial subrange)

$$\overline{[u'(r)]^2} = \frac{3C_2}{2} (\varepsilon r)^{2/3} \tag{13}$$

where $\sqrt{\overline{u'(r)^2}}$ is a measure of the velocity difference between two points distant from r.

Characteristic phenomena of aggregation and breakup

Aggregation. Two mechanisms are mainly involved in aggregation phenomena, the aggregation or collision rate, (β, L^3T^{-1}) and the collision efficiency (α, –). The aggregation rate β depends on both hydrodynamics and floc size. As mentioned earlier, the flocs follow the fluid motion and thus collision is induced by local velocity gradients within the fluid, in terms of rms turbulent velocity $\sqrt{\overline{u'^2(r)}}$. Consequently, the velocity gradients that should be introduced into the collision rate are the following

$$\Lambda > r > \eta \qquad \frac{\sqrt{\overline{u'^2(r)}}}{r} = \sqrt{\frac{3C_2}{2}} \left(\frac{\varepsilon}{r^2}\right)^{1/3} \tag{14}$$

$$\Lambda > \eta > r \qquad \frac{\sqrt{\overline{u'^2(r)}}}{r} = \sqrt{\frac{C_3}{2}} \left(\frac{\varepsilon}{\nu}\right)^{1/2} \tag{15}$$

The collision efficiency α depends on the physicochemical characteristics of the flocs.

Breakup and Size of Flocs in the Viscous Subrange of Turbulence. Breakup phenomena are controlled by the ratio of two basic forces

$$\frac{\text{Hydrodynamic forces}}{\text{Aggregate strength}} = \frac{\sigma d^2}{J} \tag{16}$$

where σ is the hydrodynamic stress exerted on the floc, d^2 is proportional to the projected area of the floc, and J is the aggregate strength. If the ratio of these forces is smaller than unity, the floc withstands the hydrodynamics stress. If the ratio is larger than unity, the hydrodynamic stress breaks up the floc.

If the breakup occurs in the viscous subrange, the hydrodynamic stress can be estimated according to Coufort et al. (2003)

$$\sigma = \rho\nu \frac{\sqrt{\overline{u'^2}}}{r} \tag{17}$$

Thus, to the extent that the breakup is controlled by turbulence, the maximum floc diameter is expressed as

$$d_{\max} = C\left(\frac{J}{\rho}\right)^{1/4} \left(\frac{\varepsilon}{\nu}\right)^{-1/4} \tag{18}$$

Table 1. Maximal Floc Size vs. the Dissipation Rate of the Kinetic Energy

Authors	Modeling of the Floc	$d = f(\varepsilon)$	
		$\Lambda > \eta > d$	$\Lambda > d > \eta$
Parker et al. (1972)	Heterogeneous medium	$d \propto \varepsilon^{-1/4}$	$d \propto \varepsilon^{-1/4}$
	Continuous medium	$d \propto \varepsilon^{-1/2}$	$d \propto \varepsilon^{-1}$
Kobayashi et al. (1999)	Heterogeneous medium	$d \propto \varepsilon^{-1/4}$	$d \propto \varepsilon^{-1/4}$
Tambo and Ozumi (1978)	Heterogeneous medium	$d \propto \varepsilon^{-0.35}$	$d \propto \varepsilon^{-0.45}$
Tomi and Bagster (1978)	Continuous medium	$d \propto \varepsilon^{-1/2}$	d is independent of ε
Matsuo and Unno (1981)	Fluid particle	$d \propto \varepsilon^{-1/2}$	$d \propto \varepsilon^{-1}$
Thomas (1964)	Continuous medium	$d \propto \varepsilon^{-1/2}$	$d \propto \varepsilon^{-5/2}$

It must be emphasized that the local dissipation rate is not uniformly distributed in the tank. In a mixing tank, the global circulation induces periodic crossing of fluid particles through the impeller region, where the dissipation rate is maximal. Because aggregation kinetics is much lower than breakup kinetics, the largest flocs will be calibrated in the regions of high dissipation rate.

Review of previous studies concerning d(ε)

The relation between the maximal floc diameter and the dissipation rate of the kinetic energy has been widely studied in the past. Two different approaches are considered for estimating the breakup. (1) The first approach considers the floc as a heterogeneous (granular) medium, composed of a finite number of attached primary particles. Following this approach, the breakup occurs when the hydrodynamic forces exceed the cohesion force of each primary particle. (2) The second approach considers the floc as a continuum medium. In this case, the floc will be broken if the hydrodynamic stress becomes larger than the cohesion stress ($\sigma > \tau_{crit}$). This choice leads to different variations in the floc diameter vs. the dissipation rate of the kinetic energy.

The Floc as a Heterogeneous Medium. Parker et al. (1972) studied two different breakup mechanisms: the surface erosion and the breakup into two or three fragments. For the second mechanism, two spheres separated by a rigid filament model the flocs, and filament breakup is assumed to occur. Thus, Parker et al. (1972) found that the maximal floc diameter is linked to the dissipation rate of the kinetic energy according to $d \propto \varepsilon^{-1/4}$, whatever the floc size in relation to the Kolmogorov microscale. Kobayashi et al. (1999) modeled the floc as a heterogeneous medium, composed of a finite number of primary particles. They found the same result as did Parker et al. (1972). The expressions of Tambo and Ozumi (1978) are slightly different because they considered the floc fractal dimension. In the viscous subrange, they related the maximal floc diameter to the dissipation rate of the kinetic energy according to $d \propto \varepsilon^{-a}$, where $0.33 < a < 0.38$. In the inertial subrange, the relation is given by $d \propto \varepsilon^{-b}$, where $0.4 < b < 0.5$.

The Floc as a Continuum Medium. Considering the floc as a continuum medium, the floc breakup occurs when $\sigma > \tau_{crit}$. Parker et al. (1972) related the maximal floc diameter to the dissipation rate of the kinetic energy, as follows

$$\Lambda > d > \eta \qquad d \propto \varepsilon^{-1} \quad \text{(inertial subrange)} \qquad (19)$$

$$\Lambda > \eta > d \qquad d \propto \varepsilon^{-1/2} \quad \text{(viscous subrange)} \qquad (20)$$

In this case, the floc breakup is attributed to turbulent pressure fluctuations. Matsuo and Unno (1981) obtained the same results. Thomas (1964) related the floc breakup to pressure fluctuations and obtained the same results as those of Parker et al. (1972) for the viscous subrange. For the inertial subrange, Thomas (1964) found that the floc diameter is related to the dissipation rate of the kinetic energy as $d \propto \varepsilon^{-5/2}$. Tomi and Bagster (1978) considered that the floc breakup is the result of local velocity gradients in the viscous subrange, meaning that, referring to Eq. 15, the floc diameter would become independent of the dissipation rate of the kinetic energy. In the inertial subrange, they considered that the floc breakup is attributed to pressure fluctuations; their analysis leads to the same result as that obtained by Parker et al. (1972): $d \propto \varepsilon^{-1}$. Table 1 summarizes the overall results concerning the variation of floc size with the dissipation rate of the kinetic energy.

The experimental apparatus will first be presented (standard vessel, A310 foil impeller and Rushton turbine). Because flocculation and hydrodynamics are strongly related, the main hydrodynamic results on the flow generated by a A310 foil impeller and a Rushton turbine in a standard vessel are presented (Bugay, 1998; Escudié, 2001). Experiments were then conducted with the two different impellers in the same standard vessel. First, the influence of the impeller type on average floc size and floc size distribution is analyzed. Then, the influence of floc history and initial flocs size distribution on floc size is studied. Differences between the two impellers on flocculation are explained, in terms of local hydrodynamic parameters. The kinetics of aggregation and breakup are outside the scope of the present study. It is assumed that after a given mixing time, a steady state between aggregation and breakup has been reached.

Experimental Methods

Perikinetic flocculation in a jar test

In these experiments, a synthetic suspension of bentonite is used to simulate the behavior of particles present in natural water. These particles are placed in demineralized water to prevent destabilization before the injection of the coagulant. The experiments on floc size distribution were carried out in a standard mixing tank of 70 L. In the tank, the concentration of bentonite is fixed at 30 mg/L. To enhance flocculation of the bentonite, it is necessary to use a chemical coagulant. In this case, aluminum sulfate hydrate [$Al_2(SO_4)_3 \cdot 14H_2O$] was chosen. As mentioned previously, mixing conditions are important in inducing an efficient dispersion of the coagulant throughout the tank, to destabilize colloid particles of bentonite. For these

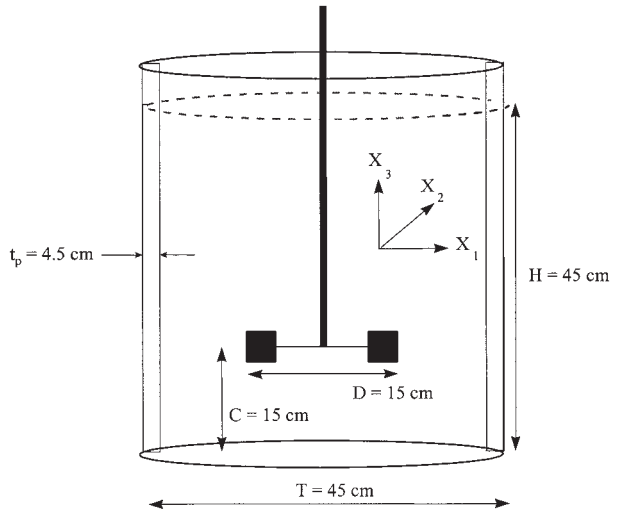

Figure 1. Standard tank.

reasons, the coagulant was injected into a small-volume tank (jar test of 1 L) under high impeller velocity. In the small-volume tank, the concentration of bentonite is then 2.1 g/L. The impeller velocity is fixed at 150 rpm for 180 s. Then, this concentrated solution is poured into the larger tank. The impeller velocity in the larger tank is fixed for each type of impeller to carry out the experiments at the same global velocity gradients.

Because demineralized water is used, the injection of aluminum sulfate hydrate as a coagulant acidifies the solution, its pH approaching 3.5. Such a pH enables strong alum flocs to be formed, which will reach Kolmogorov size.

Tank and impellers

The apparatus used in this study consists of a standard cylindrical tank equipped with a Rushton turbine or with an A310 Lightnin foil impeller (Figure 1). The cylindrical tank is made of glass (6 mm thick) with a diameter $T = 450$ mm and a liquid height $H = T = 450$ mm. The cylindrical vessel is placed in a cubic tank filled with tap water to minimize optical refraction. Four equally spaced baffles made of glass (width $B = 45$ mm $= T/10$) are fitted along the internal surface of the vessel. The tank, filled with tap water as working fluid, is open at the top. The volume (V) of liquid in the tank is 70 L.

The Rushton turbine and the A310 Lightnin foil impeller are of standard design with a diameter $D = T/3 = 150$ mm. The clearance C is equal to the impeller diameter and is measured between the bottom of the mixing vessel and the impeller disk plane. Concerning the Rushton turbine, the blade height w is $0.2D$. Both the blade thickness t_b and the disk thickness t_d are equal to 2 mm.

Image acquisition and processing

The principle of this technique consists in acquiring instantaneous two-dimensional (2-D) fields. The technique is based on the following steps:

(1) Illuminating a slice of the flow field with a light sheet to visualize flocs.

(2) Recording the image of the flocs using a digital CCD camera.

(3) Processing the images by the image-analysis software VISILOG 5. This technique is applied to the complete image from the camera to get the instantaneous floc size distribution. The system used includes a laser (Mini Yag, 15 Hz, 30 mJ), a recorder camera (Kodak Megaplus ES 1.0, 1008 $\times$ 1018 pixels), and dedicated software (VISILOG 5).

Validation

The first step of the study consists in validating the image acquisition and processing techniques. To achieve this validation, calibrated spheres of glass were used. Their size corresponds to the order of magnitude of bentonite floc size, between 100 and 500 μm. The glass spheres are manufactured industrially by crushing (not by grinding), which leads to relatively large size distribution of particles. Additional sifting must be done to obtain a controlled size of particle with a diameter between 300 and 315 μm.

During image processing, the 2-D sheet generated by the laser beam passes through the illuminated object. If the laser sheet is much thinner than the individual sphere, the area determined by the image-analysis software represents the area cut by the sheet. If the object under consideration is a perfect sphere with a diameter d, the projected area determined by this technique continuously varies from 0 to $\pi d^2/4$.

The laser beam must thus be very narrow compared to the particle dimension and the laser beam power must be adapted according to the nature of the illuminated particles. In this scope, first experiments were performed under low laser beam power (Figure 2a). In this case, the experimental diameters evolution closely matches the theoretically predicted values (Bouyer, 2002), even if a small number of particles is detected larger than particle size. In a second experiment, increasing the laser beam power leads to an overestimation of the particle size (Figure 2b). Thus, it is important to take care to use low-powered laser beams because a high-powered beam "overilluminates" the particle and results in overmeasuring the actual particle diameter.

The first conclusion from these results is that the laser power must be low to correctly estimate the size of the glass spheres. This problem will be less pronounced with the flocs because they are less reflective.

The second conclusion is that, without any more treatment, it is difficult to exploit the data because the image processing gives a large distribution of sizes corresponding to all the possible intersections between the plane and a sphere, whereas it is the size of the projected area of the sphere that is important.

Consequently an additional treatment has to be included in the image processing. Within each image only the particles whose intersection with the laser plane is maximum will be validated. This is performed by analyzing the contour of the particle: if the contour is well defined without any shading, the particle data are retained in the treatment; if the contour of the particle is shaded with different gray scales, the particle data are rejected.

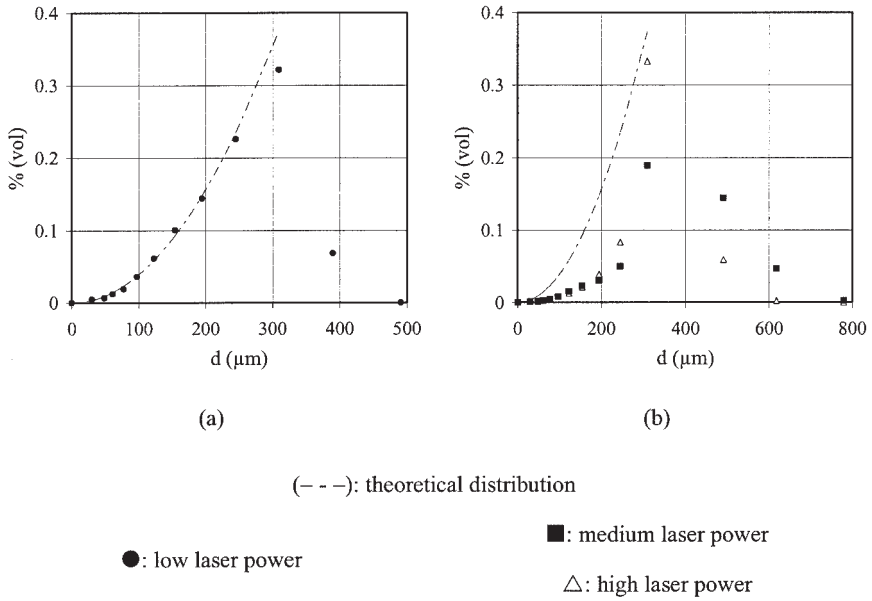

Figure 2. Experimental and theoretical variations of particle size-particle diameter between 300 and 315 μm.

Results

Hydrodynamics

The particle image velocimetry (PIV) technique has been used in the past to analyze the local hydrodynamics generated by a Lightnin A 310 axial impeller (Bugay, 1998; Bugay et al., 2002) and then by a Rushton turbine (Escudié, 2001; Escudié et al., 2003). The PIV system used is the commercial system acquired from Dantec Measurement Technology (Copenhagen, Denmark). The goal of these studies was to determine the local flow structure in terms of mean velocity fields and fluctuations. In fact, different types of motion can coexist in a mechanically agitated tank: the mean flow (or global circulation), the periodic fluctuations (or trailing vortices) induced by the blade rotation in the impeller region, and the turbulent fluctuations (which dissipate the kinetic energy).

Rushton Turbine. These three kinds of motion were estimated from experimental data by performing a triple decomposition of the velocity. The mean velocity, the periodically induced stress tensor, and the Reynolds stress tensor were analyzed in the agitated tank, close to the impeller. These data were useful in identifying and quantifying the transfer of kinetic energy between mean flow, periodic flow, and turbulence. Based on these data, the estimation of the dissipation rate of turbulent kinetic energy (TKE) was derived from the balance equations of TKE (Escudié et al., 2003). Experiments were conducted at a single value of impeller rotational speed N = 150 rpm ($G = 300\ s^{-1}$). An encoder, mounted on the impeller shaft, enabled the velocity field measurement with one of the six blades of the impeller to be synchronized. PIV provided instantaneous velocity fields in one plane.

In this study, the three components of the velocity vector and the six components of each stress tensor were measured. Moreover, it was necessary to calculate the gradient of these components in the three directions in space. As a consequence, three kinds of PIV measurement planes were studied:

(1) A vertical "radial" plane to calculate the components and their gradient in the plane.

(2) Vertical "tangential" planes to calculate the components and their gradient in the plane. Two successive planes are 5 mm apart.

(3) Horizontal planes to calculate the components and their gradient in the plane. Two successive planes are also 5 mm apart.

Consequently, experimental data are available in a vertical plane with the radial location ranging between r/R of 1.06 and 1.6, and with a normalized axial direction ranging between $2z/w$ of -1.3 and 1.3.

The order of magnitude of the Taylor microscale λ ranges between 0.45 and 1 mm. This order of magnitude corresponds to the spatial resolution of the current experiments (the size of interrogation area is 1.1×1.1 mm^2 and a vector is measured each 0.55 mm).

In the experiments, data acquisitions were synchronized with the position of impeller blades to perform the triple decomposition. The Rushton turbine is a six-blade impeller, in which the blades were equally spaced. As a consequence, given 1° angle–resolved measurements, it was necessary to perform 60 planes to reconstruct the flow between two successive blades.

The main conclusions given by Escudié et al. (2003) are recalled here. In the impeller stream jet, the main characteristic is that the kinetic energy is exchanged from the mean motion to the turbulent and organized motions. A significant amount of kinetic energy is transferred from the organized motion to the turbulent motion. The transfer of kinetic energy between organized and turbulent flow is located in a region close to the trailing vortices. Once the transfer of kinetic energy had been quantified, the balance equations of kinetic energy of mean flow, organized structure, and turbulence were analyzed in detail.

Concerning the kinetic energy of the mean flow, the viscous dissipation was calculated directly from the mean velocity gradient and found to be negligible. Concerning the organized flow, the viscous dissipation was estimated from experiments and was also negligible. Concerning the turbulence, the trans-

port of turbulent kinetic energy by the mean flow is significant in the impeller jet. It was estimated that 15% of the energy generated by the Rushton turbine is dissipated in the volume of measurement.

These data enable the distribution of dissipation rate of turbulent kinetic energy and the Kolmogorov microscale in the region of the impeller to be estimated. These data will be useful in the discussion of the results.

Lightnin A310 Axial Impeller. In the case of the hydrofoil impeller (Lightin A310, Chemineer HE-3, Moritz HAS), the blades are well designed to reduce drag at the leading edges and, therefore, to provide a high degree of axial flow with minimal power consumption. In the case of the Lightnin A 310 impeller used in turbulent regime, the impeller induces axial flow with weak trailing vortices: the phase-averaging process is thus not necessary because the magnitude of periodic fluctuation is low compared to that of a turbulent one. A simple Reynolds decomposition is shown to be sufficient.

Experiments were carried out by Bugay et al. (2002) at a single value of impeller rotational speed $N = 150$ rpm ($G = 110\ s^{-1}$).

To estimate both mean values and turbulent fluctuations, measurements were carried out for a large number of images to determine the three components of the instantaneous velocity field in a vertical plane of the tank. The size of each image is 60×48 mm. The whole plane located below the impeller was investigated ($0 < x_1 < R_{tank} = 22.5$ mm in the radial direction; $0 < x_3 < Y = 145$ mm in the vertical or axial direction). The number of velocity vectors in the radial direction on each image is 47, thus corresponding to one vector each 1.5 mm. Because the number of velocity vectors in the vertical direction on each image is 29, this also corresponds to one vector each 1.5 mm.

Turbulence was determined for "small" PIV measurement area, with characteristic length scales of measurement area equal to 60 mm and elementary window (or interrogation region) equal to 1.5 mm. These length scales can be compared to the integral length scale Λ and to the Taylor microscale λ. The integral length scale Λ can be estimated directly from PIV measurements. This was done, although the detailed results are not reported herein. Below the impeller, the integral length scale ranges from 5 to 10 mm. Between the impeller tip and the lateral wall, it ranges from 20 to 30 mm. The size of measurement area, 60×48 mm^2, thus seems reasonable. The Taylor microscale λ can be estimated from measurements presented in Bugay et al. (2002). The order of magnitude of the Taylor microscale λ ranges between 1 and 2 mm and then is equal to or slightly larger than the size of the elementary window.

In the study of Bugay (1998), the three components of the mean velocity field and the six components of the Reynolds stress components were determined precisely, especially in the region of the impeller. These data were used to estimate the dissipation rate of TKE, based on the balance equation of TKE. The dissipation rate of TKE was deduced from the balance of TKE after estimating advection and production terms. It was shown that the energy dissipated around the impeller represents 40% of the power input. In addition, the estimation of the vertical profile of the dissipation rate of TKE, averaged over the projected surface of the impeller, exhibits a rapid increase as the distance d from the impeller decreases.

These data enable both the distribution of dissipation rate of turbulent kinetic energy in the region of the impeller and the Kolmogorov microscale to be estimated. Once again, these data will be helpful in the subsequent analysis and will be presented below. Once the hydrodynamic data had been obtained, the flocculation stage was investigated (Bouyer, 2002).

Floc size vs. global dissipation rate of kinetic energy

Protocol. Considering that, after a given mixing time, a steady state between aggregation and breakup has been reached, image processing is performed under steady-state conditions. The size of each image is 15×15 mm^2. Because of the numerical camera characteristics, each pixel corresponds to a size of 15×15 μm^2, and thus flocs smaller than the pixel size will not be detected. To obtain reliable distribution of floc size, a large number of images is acquired. At large velocity gradients ($G = 300\ s^{-1}$), the floc size is relatively small and the number of flocs on one image is then large: in such a case, 20 images are statistically sufficient. At lower velocity gradients ($G = 5\ s^{-1}$), the floc size is relatively large and the number of flocs on one image is then small: in such a case, 150 images are necessary to obtain reliable statistical averages.

As previously mentioned, the perikinetic coagulation step is performed in a jar test (small tank with a volume of 1 L). This method ensures an efficient mixing between the coagulant and the particles in a small volume tank. In addition, the initial conditions are controlled and remain the same for both impellers. The impeller velocity is kept constant at 150 rpm for 180 s. At the end of this step, the 1-L volume is diluted in the large tank (70 L) where the velocity gradient is fixed at 5 s^{-1}. The flocs have the same history (size, shape, density) when they are subjected to the first (and lowest) velocity gradient ($G = 5\ s^{-1}$). As shown in Table 2, the corresponding angular impeller velocities are equal to 10 rpm for the Rushton turbine and 26 rpm for the A310 foil impeller.

The influence of the impeller type was studied at different velocity gradients (5, 10, 15, 50, 75, 100, 200, and 300 s^{-1}). Each velocity gradient is imposed for 15 min and the images are processed. Such steps, corresponding to increasing velocity gradient, are repeated until the highest velocity gradient (300 s^{-1}) is reached. This constitutes the first stage of the experiments. The second stage corresponds to decreasing velocity gradients from 300 to 5 s^{-1} (each velocity gradient being imposed for 15 min). A third stage is then performed with a reincreasing step of the velocity gradient from 5 to 300 s^{-1}.

Reversibility Phenomena. The average floc size is determined at the end of each 15-min period. This floc size is plotted vs. the global velocity gradient G for the A310 foil impeller and for the Rushton turbine (Figure 3). In each case, the same conclusions can be drawn: during the first stage (increasing velocity gradient from 5 to 300 s^{-1}), the mean floc size gradually decreases and reaches a minimum value for the maximum velocity gradient. During the second stage, with decreasing velocity gradient from 300 to 5 s^{-1}, the average floc size increases. For each velocity gradient, the floc size is larger in the second stage than that in the first stage, especially at lower velocity gradients. During the third stage, corresponding to reincreasing the velocity gradients, the flocs size decreases again and the behavior closely follows that obtained during the second stage.

The reversibility of the aggregation–breakup phenomena is

Table 2. Hydrodynamic Parameters

G (s^{-1})		5	10	15	30	50	75	100	150	200	250	300
	ε (m^2/s^3)	2.7×10^{-5}	9.1×10^{-5}	2.2×10^{-4}	8.9×10^{-4}	2.5×10^{-3}	5.7×10^{-3}	1.0×10^{-2}	2.2×10^{-2}	4.0×10^{-2}	6.2×10^{-2}	9.1×10^{-2}
	η (μm)	439	324	261	183	142	115	100	82	71	63	58
N (rpm)	Rushton	10	15	20	32	45	60	72	94	114	132	150
	A310	26	40	53	84	119	157	190	248	301	348	396
U_{tip} (m/s)	Rushton	0.078	0.12	0.16	0.25	0.35	0.47	0.57	0.74	0.90	1.04	1.18
	A310	0.4	0.6	0.8	1.3	1.8	2.4	2.8	3.7	4.5	5.2	5.9

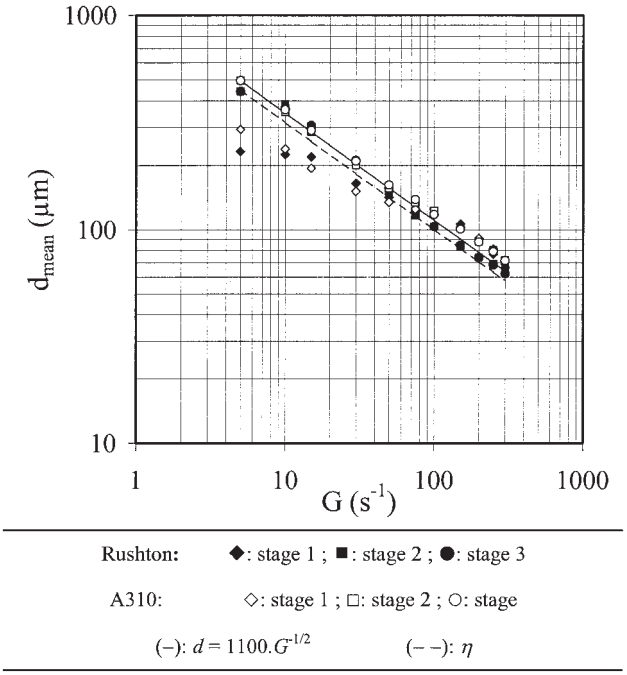

Figure 3. Average floc diameter vs. the mean velocity gradient.

observed between the second and the third stage, that is, once the flocs have been subjected to a large velocity gradient (300 s^{-1}).

Average Size vs. Global Power. In Figure 3, the variation in the average floc size vs. the velocity gradient is compared to the Kolmogorov microscale. During the first stage, the average diameter does not follow the Kolmogorov microscale. During the second and the third stages, the floc diameter follows the trend $d \propto \varepsilon^{-1/4}$, whatever the impeller type. This result is in accordance with the expected behavior based on the estimation of the ratio of forces (Eq. 16), which describes the balance between the hydrodynamic stress and the aggregate strength. The impeller type does not significantly influence the average floc size.

The average floc size is commonly used to estimate the flocculation process. However, it is not sufficient for characterizing the whole floc population. The floc size distributions are thus necessary to characterize the flocculation process. The analysis of the floc size distributions will demonstrate the influence of the impeller type. Two kinds of distributions can be reported: the floc size distributions by number and the floc size distributions weighted by size. In the first case, each entity has the same weight and the distribution represents the whole floc population. In the second case, the biggest flocs have a larger weight and the distributions primarily represent the large flocs.

In Figure 4 are reported the distributions (by number) generated with the A310 foil impeller and the Rushton turbine, during the three successive stages (increasing, decreasing, and reincreasing the velocity gradients). During the first stage (Figures 4a and d), the distribution shapes are rather similar for both impellers: for each velocity gradient, the distribution is monomodal. Once the flocs have been subjected to the highest velocity gradient (end of stage 1), the distributions correspond-

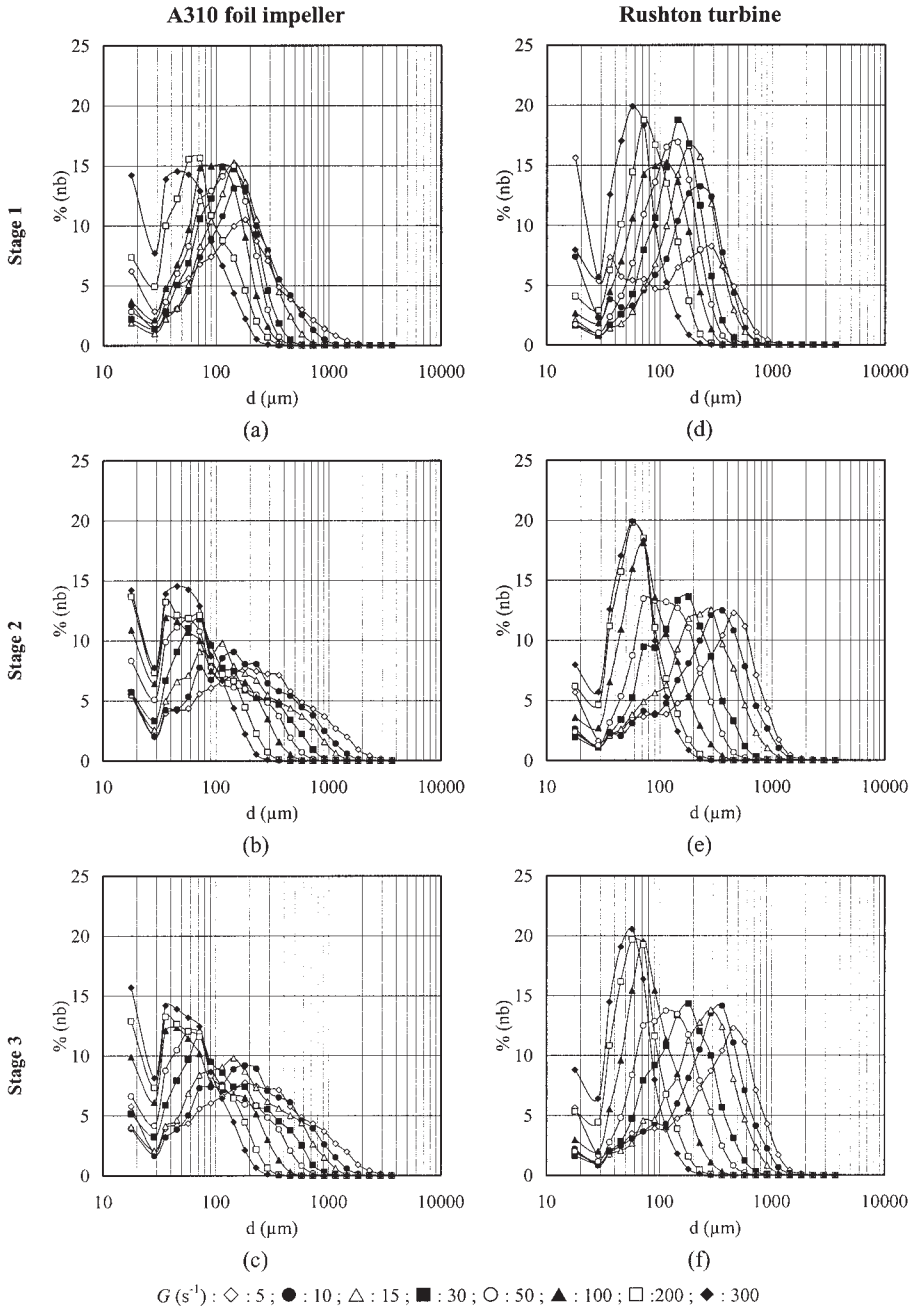

Figure 4. Floc size distributions (in number) vs. the global velocity gradient for both impellers.

ing to each impeller (during stages 2 and 3) become significantly different, even though the variations in the average floc size with the global velocity gradient are equivalent. The A310 foil impeller leads to wide distribution curves (Figures 4b and c), whereas the Rushton turbine leads to narrower distributions, indicating a most probable floc diameter (Figures 4e and f). In fact, the A310 impeller is less efficient in terms of collision rate, implying small flocs. At the same time, the A310 impeller creates larger flocs than does the Rushton turbine. It thus seems that both the collision rate and the breakup rate are significantly different with the two impellers.

The A310 foil impeller gives wide distributions of floc size (by number) and does not allow a most probable floc diameter to be defined. The most probable floc diameter is thus plotted only for the Rushton turbine vs. the global velocity gradient in Figure 5. This diameter decrease with increasing the velocity gradient. It is correlated to the Kolmogorov microscale. This result is in accordance with the analysis of Akers (1987), Wiesner (1992), and Biggs and Lant (2000).

Nonetheless, several questions remain open. First, the kinetics have not been studied, and thus it is not certain that a steady state has been reached. Second, the influence of a hydrodynamic sequencing on the floc size and floc structure must be investigated. Indeed, the discrepancy between the floc size obtained at low velocity gradients during the stages 1 and 2–3 reveals a dependency of the floc structure on the hy-

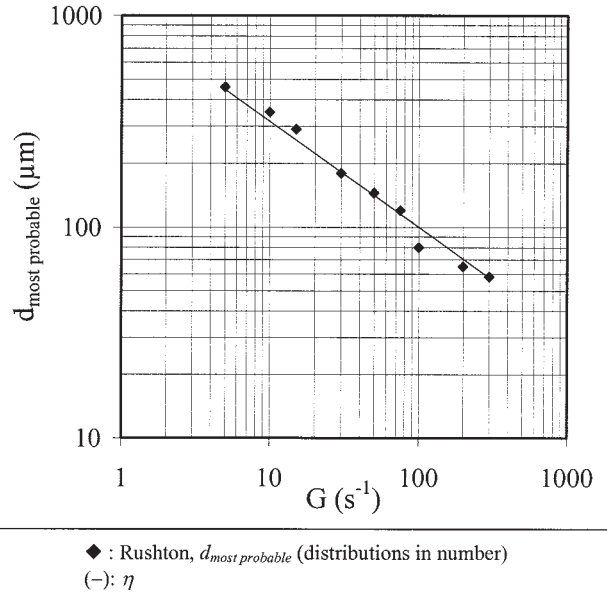

Figure 5. Most probable floc size vs. the global velocity gradient.

drodynamics: once a large velocity gradient has been imposed (stages 2 and 3), the floc sizes are slightly different. With a view to answering these questions, a complementary study was performed, based on flocculation, breakup, and reflocculation periods, each period being long enough to reach a steady state.

Flocculation, breakup, and reflocculation

The previous results showed that for a given velocity gradient, the characteristic floc size is larger during stages 2 and 3 than that during the first stage. This difference is attributed to the high velocity gradient imposed at the end of the first stage. Under this high velocity gradient, small flocs are created. These small flocs are smaller than the flocs generated in the jar test and initially injected into the tank. Under lower velocity gradients, these small flocs agglomerate to form larger flocs in stages 2 and 3 than those in stage 1, for equivalent hydrodynamic conditions. Many authors have studied this phenomenon (Clark and Flora, 1991; Clark et al., 1991; François, 1987; Lartiges, 1994; Spicer and Pratsinis, 1998). At a given velocity gradient, they showed that the average size is different after a high shear stress. Flocs with a lower porosity are created in the second aggregation stage. Clark et al. (1991) carried out two series of experiments with a soil humic acid destabilized by aluminum coagulant, for two different physicochemical conditions (pH values of 7 and 8). At the lower pH value, the floc size increases during reflocculation. On the contrary, at pH = 8, the inverse phenomenon is observed: the flocs are smaller during the reflocculation stage than those during the initial flocculation stage. At the same time, the floc structure is different: the flocs become denser. Whatever the pH value, the flocs are larger than the Kolmogorov microscale. Clark and Flora (1991) performed similar experiments with latex particles at pH 7, and found that the floc size during the reflocculation stage can be larger or smaller than the floc size during the flocculation stage, depending on the velocity gradient imposed during the breakup stage. The average floc diameter is always larger than the Kolmogorov microscale.

Spicer and Pratsinis (1998) studied the size, density, and structure of polystyrene–alum flocs. They observed that the floc size decreases during a reflocculation stage and tends to the Kolmogorov microscale if the velocity gradient imposed during the breakup stage is very high ($G = 500\ s^{-1}$). Lartiges (1994) performed two flocculation and reflocculation cycles. The flocculation and reflocculation stages were realized at $G = 60\ s^{-1}$ and the breakup stages at $G = 250\ s^{-1}$. The first experiment begins at the high velocity gradient ($G = 250\ s^{-1}$); the second one begins at the low velocity gradient ($G = 60\ s^{-1}$). A reversibility phenomenon in terms of floc size is observed in the first case: the floc size is the same between the flocculation and the reflocculation stage. In the second case, the flocs created during the first flocculation stage are smaller than the flocs created after a breakup stage. In each case, the flocs are nevertheless smaller than the Kolmogorov microscale ($\eta = 145\ \mu m$ at $G = 60\ s^{-1}$).

To analyze the phenomena observed, whatever the impeller type, new investigations were carried out.

Protocol. Flocculation is analyzed with two different impellers. Aggregation kinetics are studied for two values of the global velocity gradient (G values of 10 and 100 s^{-1}). As previously, a perikinetic stage is realized in the jar-test vessel for 180 s at 150 rpm ($G = 75\ s^{-1}$) to prepare the initial distribution of flocs. Then, the experimental protocol is divided into three stages: (1) flocculation: the flocs are poured down the tank and submitted to a low-velocity gradient (G values of 10 or 100 s^{-1}) for 90 min; (2) breakup: a very high velocity gradient ($G = 300\ s^{-1}$) is imposed for 60 min; (3) reflocculation: the initial low velocity gradient is reimposed for 150 min.

During the flocculation and the reflocculation stages, hydrodynamic conditions are the same. In addition, the physicochemical parameters remain constant. Thus, only the initial conditions are different: for the flocculation stage, the flocs come from the jar-test vessel just after destabilization, whereas for the reflocculation stage, they have undergone a very high velocity gradient ($G = 300\ s^{-1}$).

The floc size distributions are analyzed every 15 min. The duration of each step is long enough to allow a steady state to be reached.

$G = 10\ s^{-1}$. The floc size distributions are plotted in Figure 6 for each impeller and during the three stages. The distributions confirm that the steady state has been reached. During the breakup stage the distributions are similar with slightly bimodal shape, the first peak corresponding exactly to the Kolmogorov scale. It is thus clear that the turbulence controls the breakup mechanism. The distributions of floc size during the flocculation and reflocculation stages have a monomodal shape, with a peak between 200 and 250 μm for the A310 impeller, which is smaller than the Kolmogorov scale (325 μm), and between 200 and 400 μm for the Rushton turbine.

$G = 100\ s^{-1}$. The floc size distributions, represented in number, are plotted in Figure 7. During the flocculation stage, the distributions are similar in terms of shape for both impellers: the distributions have a monomodal shape, with a peak corresponding to 100–150 μm, around the Kolmogorov microscale at $G = 100\ s^{-1}$ ($\eta = 100\ \mu m$). The distributions relative to the breakup stage are very similar for each impeller,

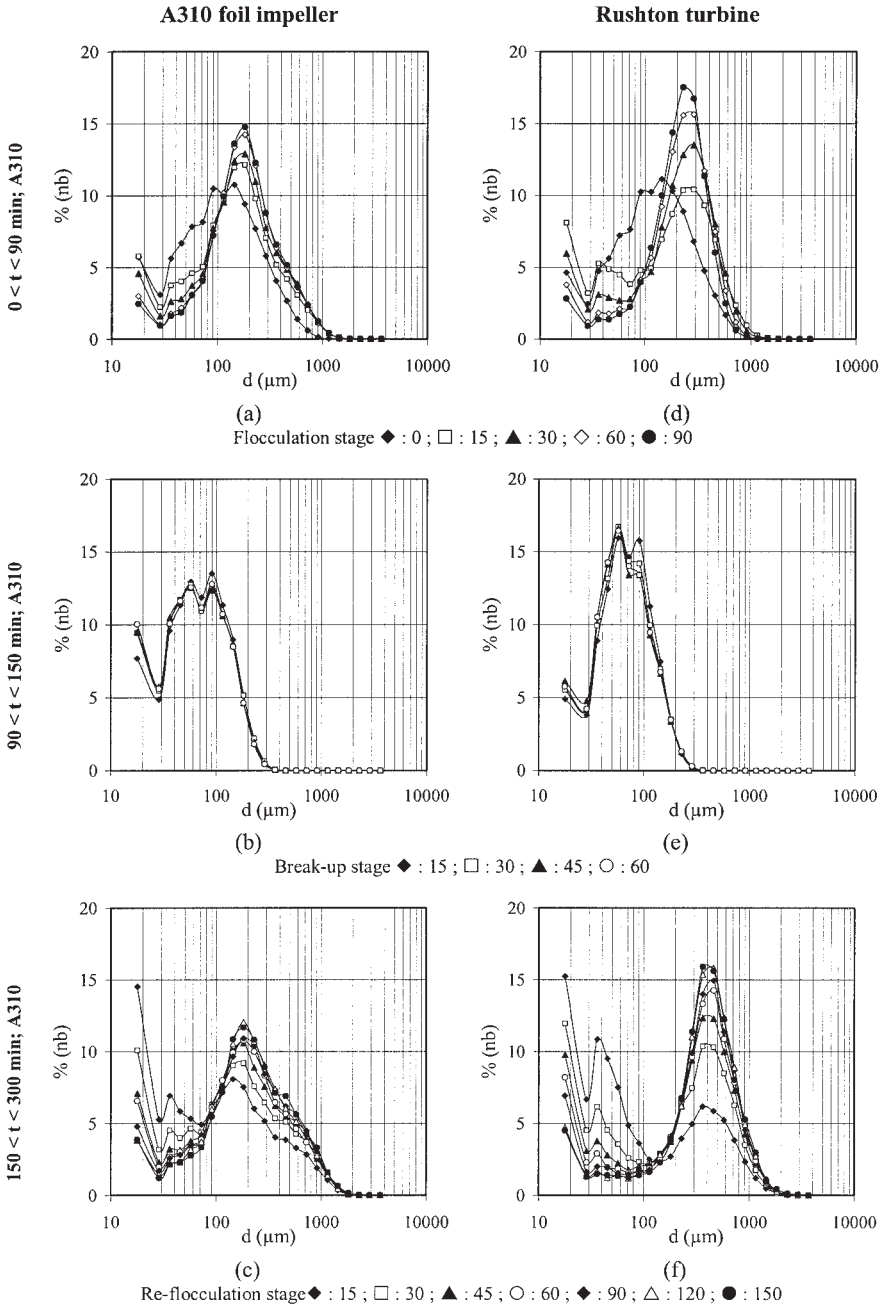

Figure 6. Floc size distributions during flocculation, breakup, and reflocculation stages at $G = 10\ s^{-1}$.

but slightly narrower with the Rushton turbine. In each case, the most probable floc diameter is about 60 μm, equal to the Kolmogorov microscale at $G = 300\ s^{-1}$ (60 μm). During the reflocculation stage, the A310 foil impeller and the Rushton turbine lead to very different floc size distributions. The distributions have a monomodal shape, with a peak corresponding to 100 μm, close to the Kolmogorov microscale, with the Rushton turbine. The A310 foil impeller leads to very wide distributions, which cannot be characterized by any peak. The floc population is composed of the same amount of particles of size between 30 and 200 μm. A large amount of flocs created during the breakup stage did not collide to form larger flocs, even after decreasing the velocity gradient from $G = 300\ s^{-1}$ to $G = 100\ s^{-1}$.

Results and Discussion

Floc size distributions

The differences in terms of the shape of distributions (Figures 7c and f) suggest that the global velocity gradient is not a sufficient parameter to model the floc population. Even though the velocity gradient is the same, the A310 foil impeller and the Rushton turbine do not create the same population of floc in the tank. This result is very interesting with respect to industrial issues. The

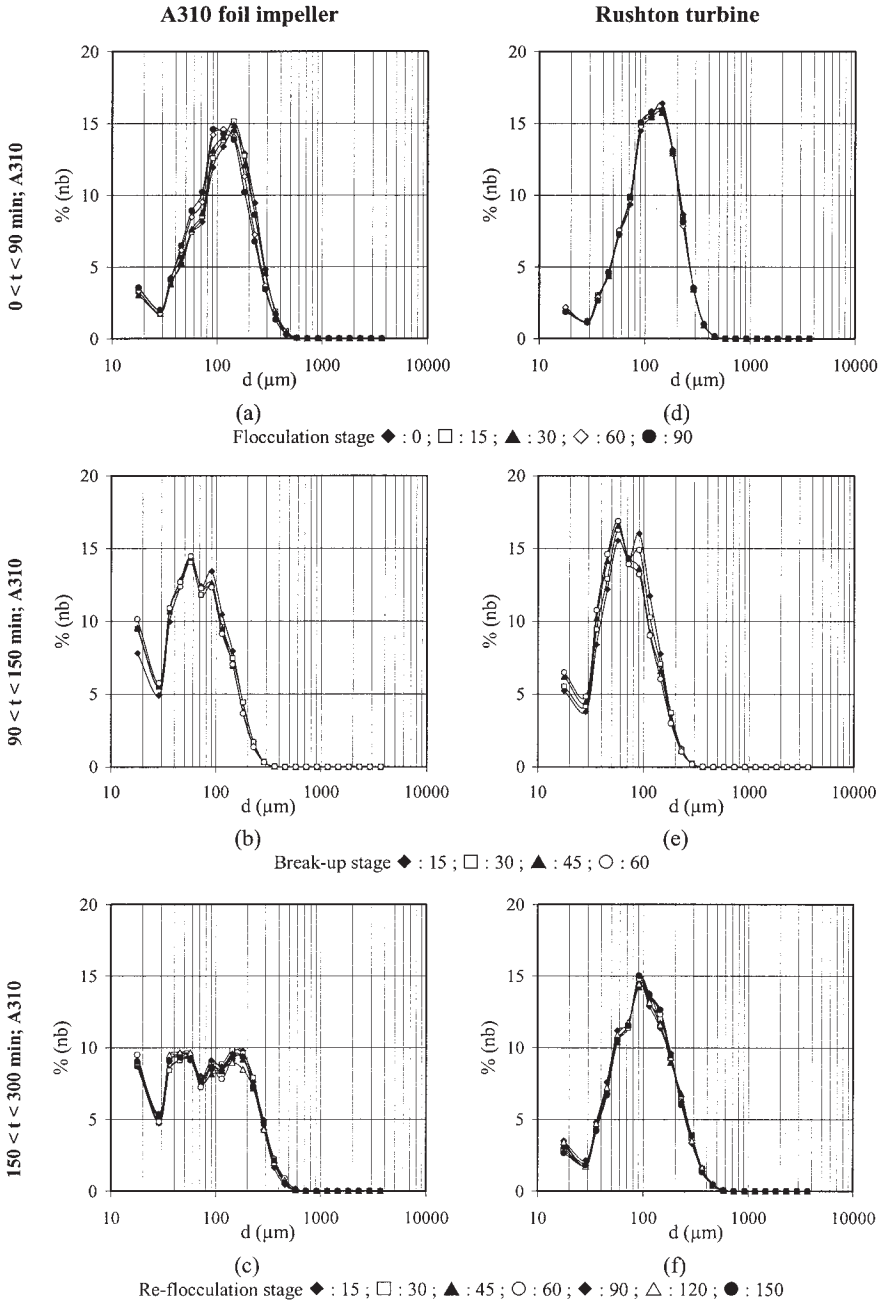

Figure 7. Floc size distributions during flocculation, breakup, and reflocculation stages at $G = 100\ s^{-1}$.

prediction of the amount of tiny particles that have not been aggregated is important in designing the downstream process.

Because the global velocity gradient is not sufficient to explain why the impellers lead to different floc size distributions, a local hydrodynamic parameter must be investigated. Ducoste et al. (1997), Bugay et al. (2002), and Escudié et al. (2003) showed that local hydrodynamics generated by the A310 foil impeller and the Rushton turbine are significantly different. In Bugay et al. (2002) and Escudié et al. (2003), the dissipation rate of TKE was estimated from experiments in the region close to the impeller. Figure 8 represents histograms of the dissipation rate of the kinetic energy and the associated Kolmogorov microscale for the two impellers, in the impeller discharge region, that is, below the impeller for the A310 foil impeller and in the jet induced by the Rushton turbine. The variables $\langle\varepsilon\rangle$ and $\langle\eta\rangle$ are normalized by global values averaged over the tank volume. The global dissipation rate is based on the power dissipated in the tank (Eq. 3). The global Kolmogorov scale is written as

$$\langle\eta\rangle = \left(\frac{\nu^3}{\langle\varepsilon\rangle}\right)^{1/4} \tag{21}$$

The experimental conditions and the hydrodynamic parameters associated with Figure 8 are shown in Table 3. Figure 8c

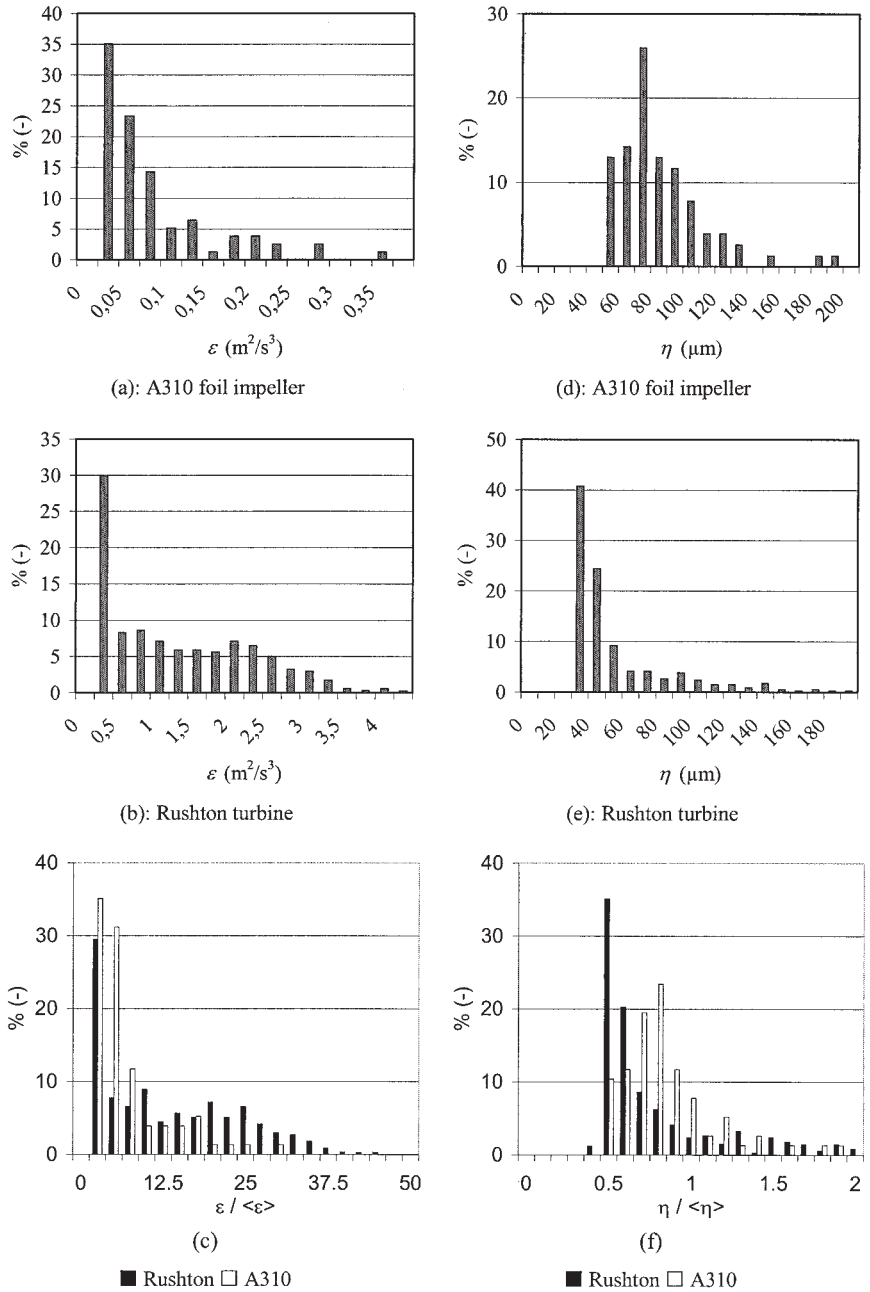

Figure 8. Dissipation rate and Kolmogorov scale in the region of the impeller.

demonstrates that the ratio of the dissipation rate of the turbulent kinetic energy in the impeller region divided by $\langle\varepsilon\rangle$, the dissipation rate averaged over the tank, has a wider distribution and higher values for the Rushton turbine than those for the A310 foil impeller. The ratio $\varepsilon/\langle\varepsilon\rangle$ is of the order of 25 with the Rushton turbine and less than 10 with the axial impeller. At the same global velocity gradient, the local value of the dissipation rate of the turbulent kinetic energy in the region of the impeller is larger with the Rushton turbine than that with the A310 foil impeller.

The local Kolmogorov microscale is determined by Eq. 6. For both impellers, the distributions of the Kolmogorov microscale in the impeller discharge zone are centered on a value slightly smaller than the average value of the Kolmogorov

Table 3. Experimental Conditions and Hydrodynamic Parameters Associated with the Hydrodynamic Studies of Bugay (1998) and Escudié (2001)

	N (rpm)	G (s^{-1})	ε_{avg} (m^2/s^3)	η_{avg} (μm)
Bugay (1998); A310 foil impeller	200	110	1.2×10^{-2}	100
Escudié (2001); Rushton turbine	150	300	9.1×10^{-2}	60

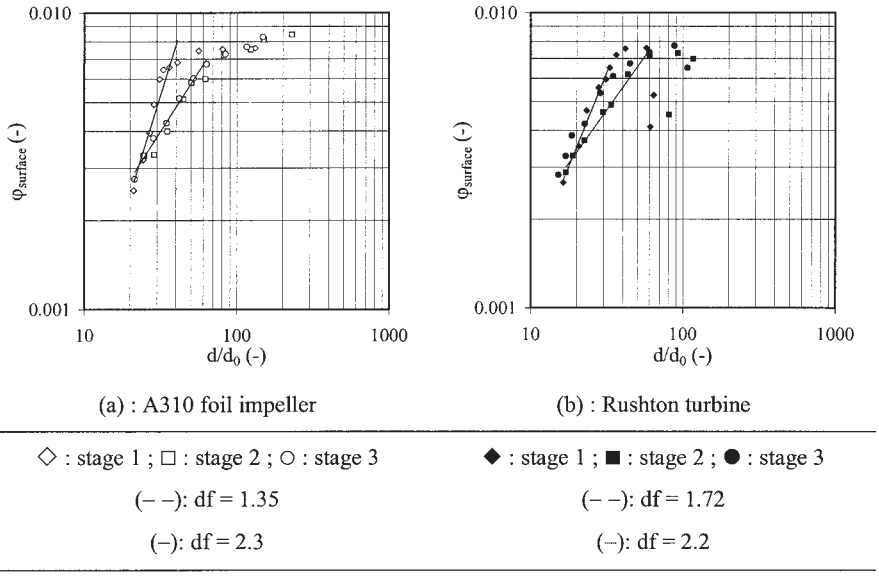

Figure 9. Variation of the surface solid fraction with time to estimate the floc fractal dimension.

microscale $\langle\eta\rangle$ given by Eq. 21. This result was expected since the total energy input in the tank is mainly dissipated in the impeller region (Bugay et al., 2002; Ducoste et al. 1997; Escudié et al., 2003) and less in the bulk region. Furthermore, the ratio of the Kolmogorov microscale in the region of the impeller divided to $\langle\eta\rangle$, the Kolmogorov microscale average over the volume of the tank, is close to 1 with the axial impeller and closer to 0.5 with the Rushton turbine. In addition, the histogram is wide with the axial impeller ($\eta/\langle\eta\rangle$ between 50 and 200% in Figure 8b) and rather thin with the Rushton turbine. If one considers that the floc size is correlated to the Kolmogorov microscale, particularly in the impeller discharge zone, the floc size distributions generated by the A310 foil impeller (Figure 7c) are wider than the floc size distributions generated by the Rushton turbine (Figure 7f).

Structure of flocs

The aggregate strength depends primarily on the physicochemical conditions. In fact, the different distributions plotted in Figures 7c and f correspond to a steady state at a constant velocity gradient ($G = 100\ s^{-1}$), with initial floc size distributions induced by a high velocity gradient ($G = 300\ s^{-1}$). The physicochemical conditions remain the same, so the aggregate strength is probably affected by the hydrodynamics. Within this framework, the structure of the flocs is analyzed.

Oles (1991) proposed to estimate the fractal dimension of flocs from the solid volume fraction. First, Oles (1991) considered that the total solid volume fraction does not vary during the flocculation process. He plotted the ratio between the solid volume fraction and the initial solid volume fraction vs. d/d_0, where d_0 represents the initial floc diameter. The slopes of the curves give the fractal dimension of the flocs.

Because the floc size presented herein is determined by image analysis, the solid surface fraction can be estimated. The average diameter of the initial particles of bentonite was determined from a Malvern Mastersizer and is close to 5 μm. Figure 9 represents the variation of the solid surface fraction with time for both impellers during stages 1, 2, and 3. During stage 1, the fractal dimensions of the flocs are estimated: 1.35 for the A310 foil impeller and 1.7 for the Rushton turbine. Once the flocs have been subjected to the high-velocity gradient ($G = 300\ s^{-1}$), the fractal dimension increases (2.3 for the A310 foil impeller and 2.2 for the Rushton turbine). This result indicates that the floc structure changes, the floc becoming denser. At a high-velocity gradient, the two impellers generate similar populations of flocs, with the same distribution and with the same structure in terms of fractal dimension.

Influence of initial conditions on floc size distributions for each impeller

The influence of the initial floc size distributions can be investigated from the flocculation, breakup, and reflocculation stages. For the flocculation stages, the primary particles come from the perikinetic coagulation stage; for the reflocculation stage, the initial distributions are formed under a high-velocity gradient, inducing strong breakup of the flocs. Figure 10 represents the initial and final floc size distributions (in number) for both flocculation and reflocculation stages. During these two stages, the velocity gradient is the same (G values of 10 and $100\ s^{-1}$). The final distributions are obtained after 90 min of flocculation and after 150 min of reflocculation. Figure 10 shows clearly that the floc size distributions created during the flocculation and the reflocculation stages, in a steady state and under the same velocity gradient, are basically different. The difference is even more significant with the Rushton turbine. Consequently, the steady-state floc size distribution for a fixed value of the velocity gradient does depend on the initial floc size distribution.

In particular, the structure of the initial flocs is probably different after the breakup stage and after perikinetic coagulation in the jar test. Clark and Flora (1991) showed that the floc structure after flocculation depends on the primary particle size.

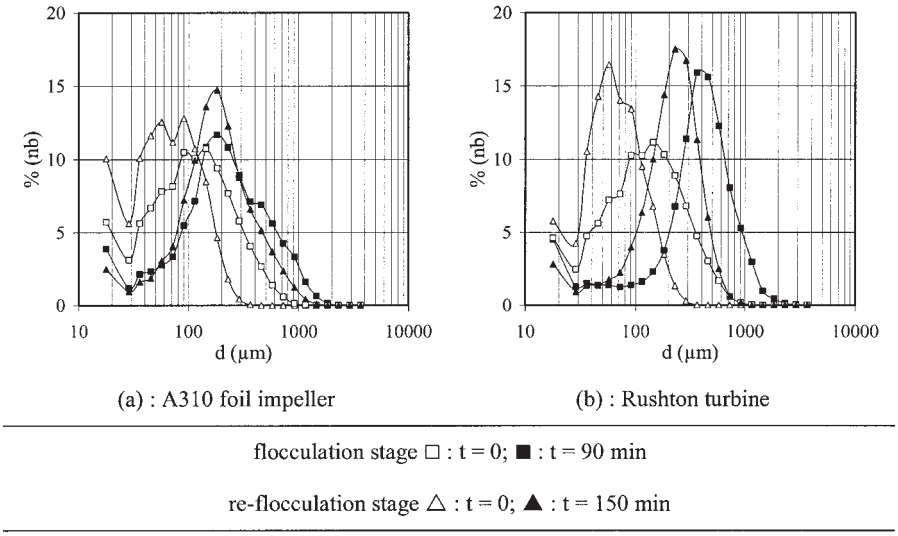

Figure 10. Influence of the initial floc size distribution on the floc size distribution after the flocculation and the reflocculation stage at $G = 10\ s^{-1}$.

Influence of impeller type on size distribution during reflocculation stage

At $G = 10\ s^{-1}$ (Figure 10), the floc size distributions of the two impellers during the reflocculation stage have similar monomodal shape. The most probable floc diameter is about 400 μm for the Rushton turbine and only about 200 μm for the A310 foil impeller. The Kolmogorov microscale is close to 325 μm. Figure 11 represents the floc size distributions during flocculation and reflocculation stages, for both impellers at $G = 100\ s^{-1}$. The initial size distributions are the same for the two impellers. The floc size distributions can be compared when a steady state has been reached during the reflocculation stage.

At $G = 100\ s^{-1}$ (Figure 11b), the Rushton turbine determines the floc size around a peak value corresponding to a most probable floc diameter close to the Kolmogorov microscale of 100 μm. The populations of the largest flocs are similar whatever the impeller type. This result indicates that the large flocs are calibrated by the smallest hydrodynamic structures (Kolmogorov scale), whose size is directly related to the power dissipated in the tank. On the contrary, the floc size distribution curves obtained with the A310 foil impeller are wide (Figure 11a). The small flocs created during the breakup stage have not been eliminated by the axial impeller, during the reflocculation stage.

The aggregation efficiency of the two impellers is then basically different. It depends on local hydrodynamics generated by each impeller. Aggregation occurs for floc sizes below the Kolmogorov scale. Thus, the velocity difference controlling the collision of two flocs must be related to the local velocity gradients in the viscous subrange. These velocity gradients are related to the local dissipation rate (Eq. 15) and are thus larger

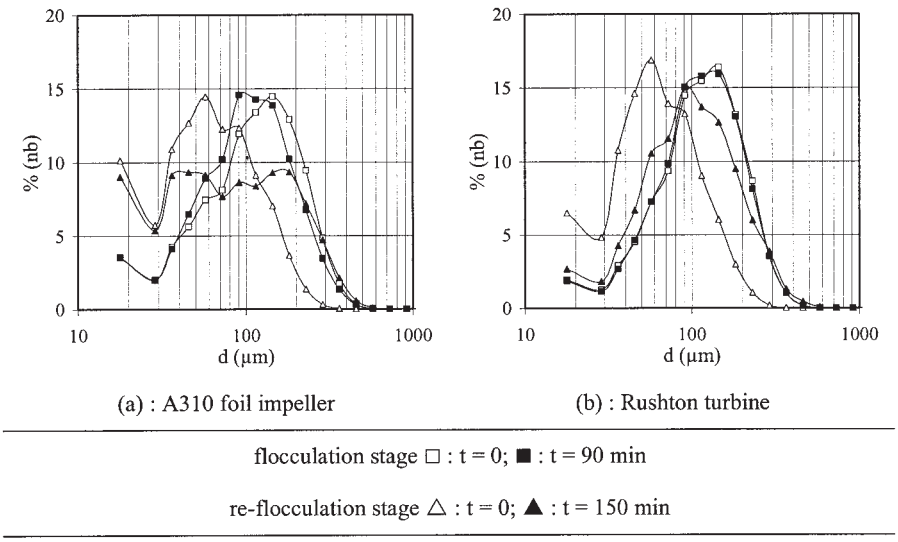

Figure 11. Influence of the initial floc size distribution on the floc size distribution after the flocculation and the reflocculation stage at $G = 100\ s^{-1}$.

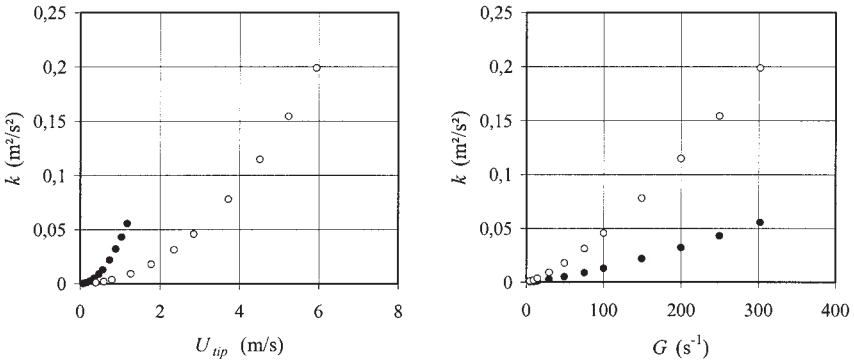

Figure 12. Turbulent kinetic energy in the impeller region.

with the Rushton turbine than with the axial impeller, at least in the region close to the impeller (Figure 8). Another phenomenon controlling the aggregation is related to the collision frequency. It seems that the flocs are trapped in the bulk of the vessel by energy-containing eddies. Then, these eddies are stretched by vortex stretching and the vortex size decreases to the Kolmogorov scale. The collision probably occurs during this vortex stretching. The eddy turnover time (given by Eq. 8) can be analyzed in terms of the characteristic time scale of the transfer of energy from large to small turbulent scales: it is thus a measure of the vortex stretching period (Baldyga and Burns, 1999). The difference in efficiency between the two impellers can be investigated in terms of eddy turnover time, which can be estimated from experiments.

Bugay et al. (2002) and Escudié et al. (2003) studied local hydrodynamics generated by the A310 foil impeller and the Rushton turbine, respectively. In the impeller region, the square root of the turbulent kinetic energy $\langle k \rangle$ is about 20% of the impeller tip velocity for the Rushton turbine but only about 7.5% for the A310 foil impeller. In addition, the dissipation rate of the turbulent kinetic energy (ε) is 10 times greater than its volume average value. For the A310 foil impeller, the dissipation rate ε is only five times greater in the impeller region than the volume average value. Figures 12a and b represent the average turbulent kinetic energy $\langle k \rangle$ in the region of the impeller vs., respectively, the impeller tip velocity and the global velocity gradient. At the same impeller velocity, the Rushton turbine generates more turbulence than does the A310 foil impeller. At a given dissipated power, the turbulent kinetic energy $\langle k \rangle$ is larger with the A310 foil impeller because the impeller velocity has to be 2.6 times greater than that with the Rushton turbine to dissipate the same amount of power in the tank. From the turbulent kinetic energy $\langle k \rangle$ and the dissipation rate of the turbulent kinetic energy $\langle \varepsilon \rangle$, one can estimate $\langle k \rangle / \langle \varepsilon \rangle$. This parameter represents the time necessary to stretch a vortex, thus to transfer energy from the large energetic vortex to the smallest dissipative vortex (Kolmogorov microscale). Figure 13 represents the eddy turnover time for both impellers. At the same global velocity gradient, the energy is transferred more rapidly with the Rushton turbine than with the A310 foil impeller. Considering that the collisions between flocs are attributed to local velocity gradients below the Kolmogorov microscale, the collision efficiency will be increased if the eddy turnover time is small. This result could explain the difference in aggregation efficiency observed with the A310 foil impeller and the Rushton turbine.

This difference in aggregation efficiency is shown to be greater at higher velocity gradients. In particular, in Figure 11, the small flocs are eliminated at $G = 10\ s^{-1}$ but are not eliminated at $G = 100\ s^{-1}$. A possible explanation is related to the size of the large flocs. At low-velocity gradient, $G = 10\ s^{-1}$, the Kolmogorov scale is large (325 μm) and thus the larger flocs are five times the scale of the flocs generated during the breakup stage (60 μm). The volume of the large flocs is then 25 times larger than the volume of the initial flocs, and thus the collision efficiency is high. At higher velocity gradient, $G = 100\ s^{-1}$, the Kolmogorov scale is lower (100 μm) and thus the larger flocs are less than two times the scale of the flocs generated during the breakup stage (60 μm). The volume of the large flocs is only five times larger than the volume of the initial flocs, and thus the collision efficiency is lower.

Conclusions

The goal of this communication was to analyze the relationship between floc size and hydrodynamics in a mixing tank, to improve the flocculation step in water treatment plants. In

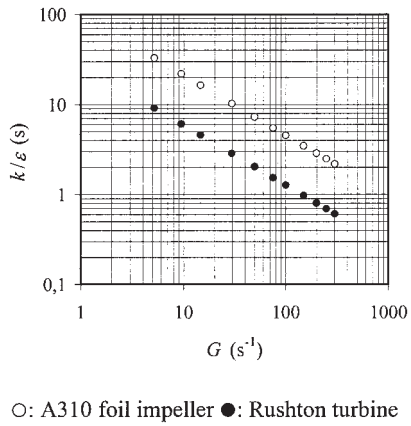

Figure 13. Stretching time for both impellers.

water treatment plants, the flocculation process is used to remove colloidal matter by chemical means. In these experiments, a synthetic suspension of bentonite was used to simulate the behavior of particles present in natural water. The experiments on floc size distribution were carried out in a standard mixing tank of 70 L. To enhance flocculation of bentonite, aluminum sulfate hydrate [$Al_2(SO_4)_3 \cdot 14H_2O$] was chosen as coagulant.

The first question addressed herein concerned the relation between the average floc size and the viscous dissipation of kinetic energy. In water treatment, the global velocity gradient is often substituted for the viscous dissipation. The basic question was to know whether the global velocity gradient was sufficient in itself to determine the characteristic size of the flocs. A first series of flocculation experiments was thus conducted in a mixing tank with two different impellers: a Rushton turbine and a Lightnin A310 axial impeller. Experiments were done with each impeller for equivalent dissipated power conditions, leading to equivalent global velocity gradients. Because the power numbers of the impellers were different, the same velocity gradient corresponds to different impeller velocities for the two impellers. Previous studies showed that the local hydrodynamics is strongly dependent on the impeller type. The present experiments on floc size by image processing demonstrate that the average floc size depends on the global velocity gradient, whatever the impeller type. More precisely, in the case of the Rushton turbine, the most probable diameter does follow the Kolmogorov microscale, expressed in terms of viscous dissipation averaged over the tank. With respect to the average floc size, the global velocity gradient is thus sufficient to characterize this size. What is especially important to emphasize is that the floc size distributions are significantly different for each impeller. The A310 foil impeller leads to wide distributions, whereas the Rushton turbine leads to narrower distributions, exhibiting a most probable floc diameter. Thus, the global velocity gradient is not sufficient to characterize the floc size distribution.

The second question addressed the dependency of the floc size on the history of mixing. A second series of experiments consisted of flocculation, breakup, and reflocculation steps. These experiments showed that the average floc size can remain similar after flocculation or reflocculation steps: reversibility phenomena of aggregation and breakup mechanisms have been demonstrated once the floc was subjected to a high velocity gradient. Moreover, these results confirmed that the floc size distributions can be substantially different with different impellers: at a high global velocity gradient (300 s^{-1}), the distribution generated by the two different impellers during the reflocculation stage are significantly different. In particular, it was shown that the aggregation efficiency was lower with the A310 impeller than with the Rushton turbine. A possible mechanism is proposed in terms of collision rate related to vortex stretching time scale.

Notation

d = floc diameter, m
D = impeller diameter, m
G = global velocity gradient, s^{-1}
H = liquid height in the tank, m
J = aggregate strength, N
k = turbulent kinetic energy, m^2/s^2
N = rotational speed, rpm
N_P = power number
P = power input, W
Re = Reynolds number
T = tank diameter, m
t_b = blade thickness, m
t_d = disk thickness (Rushton turbine), m
$\overline{u'^2(r)}$ = rms fluctuating velocity, m/s
U_{tip} = tip velocity, m/s
V = tank volume, m^3
w = impeller width, m
X_3 = axial distance, m

Greek letters

$\langle\varepsilon\rangle$ = global dissipation rate of turbulent kinetic energy, m^2/s^3
ε = local dissipation rate of turbulent kinetic energy, m^2/s^3
η = Kolmogrov scale, m
τ_K = Kolmogorov time microscale, s
τ_E = eddy turnover time, s
σ = hydrodynamic stress, Pa
λ = Taylor microscale, m
Λ = macrolength scale, m
ν = kinematic viscosity, m^2/s
ρ = fluid density, kg/m^3

Acknowledgments

The financial support provided by Society ONDEO Services is gratefully acknowledged.

Literature Cited

Akers, R. J., A. G. Rushton, and J. I. T. Stenhouse, "Floc Breakage: The Dynamic Response of the Particle Size Distribution in a Flocculated Suspension to a Step Change in Turbulent Energy Dissipation," *Chem. Eng. Sci.*, **42**, 787 (1987).

Baldyga, J., and J. R. Bourne, *Turbulent Mixing and Chemical Reactions*, Wiley, New York (1999).

Biggs, C. A., and P. A. Lant, "Activated Sludge Flocculation: On-line Determination of Floc Size and the Effect of Shear," *Water Res.*, **34**(9), 2542 (2000).

Bouyer, D., "Analyse Expérimentale de la Floculation: Influence de l'Hydrodynamique sur les Phénomènes d'Agrégation et de Rupture," PhD Thesis, Institut National des Sciences Appliquées de Toulouse, France (2002).

Bouyer, D., A. Liné, A. Cockx, and Z. Do-Quang, "Experimental Analysis of Floc Size Distribution and Hydrodynamics in a Jar-Test," *Trans. IchemE*, **79**(Part A), 1017 (2001).

Bugay, S., "Analyse Locale des Échelles Caractéristiques du Mélange: Application de la Technique P.I.V. aux Cuves Agitées," PhD Thesis, Institut National des Sciences Appliquées, Toulouse, France (1998).

Bugay, S., R. Escudié, and A. Liné, "Experimental Analysis of Mean Flow and Turbulence Structure in Agitated Tank Based on PIV Technique with Axial Impeller," *AIChE J.*, **48**(3), 463 (2002).

Clark, M. M., and J. R. V. Flora, "Floc Restructuring in Varied Turbulent Mixing," *J. Colloid Interface Sci.*, **147**, 407 (1991).

Clark, M. M., J.-M. Laîné, M. R. Wiesner, and J. Mallevialle, "Hydrodynamic Conditioning of Aluminium–Humic Acid Floc," *Fluid/Particle Sep. J.*, **4**(3), 154 (1991).

Coufort, C., and A. Liné, "Force and Stress Distribution of Spherical Particles: Application to Flocs Break-up," *Trans IChemE*, **81**, Part A, 1206 (2003).

Duscoste, J. J., M. M. Clark, and R. J. Weetman, "Turbulence in Flocculators: The Effect of Tank Size and Impeller Type," *AIChE J.*, **43**, 328 (1997).

Escudié, R., "Structure Locale de l'Hydrodynamique Générée par une Turbine de Rushton," PhD Thesis, Institut National des Sciences Appliquées, Toulouse, France (2001).

Escudié, R., and A. Liné, "Experimental Analysis of Hydrodynamics in a Radially Agitated Tank," *AIChE J.*, **49**, 585 (2003).

François, R. J., "Strength of Aluminium Hydroxide Floc," *Water Res.*, **21**, 1023 (1987).

Hinze, J. O., *Turbulence: An Introduction to Its Mechanism and Theory*, 1st Edition, McGraw Hill, New York (1959).
Hounslow, M. J., "A Discrete Population Balance for Continuous Systems at Steady State," *AIChE J.*, **34**(11), 1821 (1988)
Kobayashi, M., Y. Adachi, and S. Ooi, "Breakup of Fractal Flocs in a Turbulent fLow," *Langmuir*, **15**, 4351 (1999).
Lartiges, B., "Déstabilisation d'une Suspension de Silice Colloïdale par un Sel d'Aluminium Relations entre les Phénomènes de Surface, la Structure et la Granulométrie des Flocs," PhD Thesis, Institut National Polytechnique de Lorraine, France (1994).
Matsuo, T., and H. Unno, "Forces Acting on Floc and Strength of Floc," *J. Environ. Eng. Div.*, **107**, EE3 (1981).
Obukhoff, A. M., and A. M. Yaglom, *Prikl. Matematika Mekhanika*, **15**, 3 (1951).
Oles, V., "Shear-Induced Aggregation and Breakup of Polystyrene Latex Particles," *J. Colloid Interface Sci.*, **154**, 351 (1992).
Parker, D. S., W. J. Kauffman, M. Asce, and D. Jenkins, "Floc Break-up in Turbulent Flocculation Processes," *J. Sanitary Eng. Div.*, 79 (1972).
Spicer, P. T., and S. E. Pratsinis, "Coagulation and Fragmentation: Universal Steady-State Particle Size Distribution," *AIChE J.*, **42**, 1612 (1988).
Spicer, P. T., S. E. Pratsinis, J. Raper, R. Amal, G. Bushell, and G. Meesters, "Effect of Shear Schedule on Particle Size, Density, and Structure during Flocculation in Stirred Tanks," *Powder Technol.*, **97**, 26 (1998).
Tambo, N., and H. Hozumi, "Physical Characteristics of Flocs—II. Strength of Floc," *Water Res.*, **13**, 421 (1978).
Thomas, D. G., "Turbulent Disruption of Flocs in Small Size Suspension," *AIChE J.*, **10**, 517 (1964).
Tomi, D., and D. F. Bagster, "The Behaviour of Aggregates in Stirred Vessel. Part I—Theoretical Consideration on the Effects of Agitation," *Trans. IChemE*, **56**, 1 (1978).
Wiesner, M. R., "Kinetics of Aggregate Formation in Rapid Mix," *Water Res.*, **26**(3), 379 (1992).

Manuscript received Feb. 20, 2003, revision received Nov. 24, 2003, and final revision received Apr. 29, 2004.